Vol. 15, No. 43, Summer 2025, pages 21-30

Journal of Analytical and Numerical Methods in Mining Engineering

Journal home page: http://anm.yazd.ac.ir/

Research article

Three-Dimensional Analysis of Seepage in Fractured Rock Masses and Evaluation of the Accuracy of Empirical Methods for Predicting Permeability in Cutoff Walls: A Case Study of Chamshir Dam

Alireza Baghbanan[1*], Masoud Dararbi[1], Amirhosein Momeni[1], Ahmad Rahmani Shahraki[1], Amin Azhari[1]

1- Dept. of Mining Engineering, Isfahan University of Technology, Isfahan, Iran

*Corresponding author: E-mail: *bagh110@iut.ac.ir*

*(*Received*: November 2024*, Accepted*: April 2025)*

DOI: 10.22034/ANM.2025.22475.1654

Keywords

Rock Mass Permeability

Seepage Control

Cutoff Wall

Numerical Seepage Modeling

3DEC

Seep/w

Abstract

The assessment of the permeability of fractured rock formations plays a crucial role in optimizing the design of impermeable layers in dam construction projects. Uncontrolled seepage and deficiencies in the preparation of dam foundations and abutments are among the primary causes of dam failures. This study focuses on the investigation of the permeability of fractured rock masses and the design of a cutoff wall using numerical modeling techniques. The fracture network was modeled using the discrete element method (DEM) in the 3DEC software, considering the joint patterns specific to the region. Geological conditions were incorporated into the three-dimensional model to enhance its realism and accuracy. The numerical model was validated by comparing its results with data obtained from Lugeon tests, ensuring the reliability of the simulations. The cutoff wall was designed in accordance with the geological and hydrogeological conditions of the site. The performance of the cutoff wall was analyzed by modeling two scenarios: one with the cutoff wall and the other without it, using the 3DEC and Seep/w software. Results from the seepage analyses conducted using these software tools showed that the implementation of the cutoff wall reduced seepage by 70% according to 3DEC and 80% according to Seep/w. Additionally, the permeability values obtained through various empirical methods were compared, and their errors were evaluated using the Root Mean Square Error (RMSE) index. The obtained RMSE values for the methods are as follows: Dupuit (0.2× 10^-7), Altovsky (1.1× 10^-7), Moye (0.18 × 10^-7), Hoek-Bray (0.15 × 10^-7), and Verigin (0.1 × 10^-7), respectively. The findings revealed that the Hoek method and Verigin method provided the most accurate results, exhibiting the least amount of error when compared to other empirical methods.

1. INTRODUCTION

The assessment of seepage in dams is critically important for addressing water leakage from foundations and abutments, as well as its impact on the stability of dam structures and their economic feasibility. Uncontrolled seepage or inadequate preparation of dam foundations and abutments has been reported as the main cause of numerous dam-related leakage problems and failures, with 30% of all failures attributed to seepage issues [1]. Consequently, extensive studies have been conducted to determine the extent and areas of seepage in dam abutments and to control it based on the hydrogeological conditions of dam sites, equivalent media theory,

numerical methods, and empirical approaches [2-6].

Li et al. [7] developed a back-analysis model for evaluating the permeability of dam foundations that had been overlooked during design. This model, which employed finite element methods and neural networks, identified potential leakage pathways and assessed seepage flows in dam foundations and abutments. Jiang et al. [8] performed a three-dimensional transient numerical simulation of seepage based on a regional groundwater flow model. They calculated seepage quantities under natural and reservoir impounding conditions, with and without a cutoff wall. Their study produced a detailed three-dimensional model of the groundwater flow system, where permeability parameters and precipitation infiltration rates were calibrated through inverse modeling.

Gao et al. [9] conducted numerical simulations using an equivalent continuum model to analyze the seepage behavior of a dam in China. Their findings indicated that cracks in the surface and varying degrees of damage to the cutoff wall significantly influenced seepage patterns. Zhang et al. [10] proposed a systematic approach for optimizing the design and evaluation of seepage control measures in reservoir dams under karst conditions. They utilized a three-dimensional equivalent continuum finite element model to examine the effectiveness of proposed and optimized seepage control measures. Kheiri et al. [11] investigated the effects of cutoff walls and horizontal drains on the hydraulic gradient and uplift pressure beneath an earth dam. Their study also considered the impact of the position and depth of cutoff walls on seepage beneath the dam. Aghajani et al. [12], using the Seep/w software, conducted a comprehensive analysis of the optimal placement of cutoff walls and the effectiveness of horizontal drainage in reducing seepage flows from earth dams. Sazzad et al. [13] focused on the effect of grout curtains on seepage characteristics in earth dams with permeable and impermeable foundations.

Torabi Haghighi et al. [14] developed a novel approach to quantify the efficiency of seepage control measures in earth dams based on a combination of seepage modeling and monitoring data. Moharrami et al. [15] explored the performance of cutoff walls in mitigating uplift pressure beneath hydraulic structures, evaluating the influence of wall inclination on seepage behavior. Zhao and Jiang [16] experimentally assessed seepage characteristics of fractured rock masses and their correlation with permeable media. They proposed an innovative evolutionary equation for permeability that accounts for creep damage.

Zarif Sanayei and Javdanian [17] provided an analytical evaluation of seepage from dams, addressing uplift pressure and asymmetrical boundary conditions. Their study introduced new two-dimensional and three-dimensional analytical solutions for steady-state seepage beneath dams with non-symmetric boundary conditions.

Several studies have utilized empirical models for seepage analysis, including the Hele-Shaw model, permeability tank tests, and the Altovski model [18-22]. One notable example is the use of the Hele-Shaw model to experimentally assess the effects of internal grout curtains on seepage through earth dams. This research aimed to determine the effectiveness of cutoff walls in preventing water leakage and the influence of their position on seepage discharge and head loss [23]. Due to the complexity of seepage conditions at dam sites, the results of different analyses—even for the same project and initial data—can vary significantly. Ensuring that the computed results accurately reflect engineering reality is not only crucial for analyzing dam seepage but also for comparing and optimizing designs. Seepage analysis and control remain critical aspects of dam design, directly affecting both the safety and economic viability of projects [4, 24]. However, only a limited number of studies have focused on the use of engineering data to optimize seepage control designs, identify theoretical computation methods, generalize models, define computational boundaries, and establish realistic seepage engineering properties through calculation and analysis [7, 25-29].

The objective of this study is to develop a three-dimensional model to predict seepage rates in dam abutments, design a cutoff wall, and evaluate its effectiveness. Additionally, given the existence of numerous empirical methods for estimating permeability—each yielding different results—this study aims to evaluate the errors associated with these methods. Considering the aforementioned challenges with empirical methods and the capability of numerical simulations to closely approximate real-world conditions, this study employs discrete element and finite element methods using the 3DEC and Seep/w software environments for seepage modeling and analysis.

2. GEOLOGICAL CHARACTERISTICS OF THE FIELD

The Chamshir Dam, located 35 kilometers south of Gachsaran city in Iran, is built on the

Mishan Formation, which serves as its primary foundation. The area's geology features resistant units like limestone and sandstone in elevated regions, while lower areas consist of weaker formations such as marl and gypsum, influenced by the Gachsaran and Mishan formations. The Mishan Formation, dating to the Early to Middle Miocene, comprises gray marlstone, shell-bearing clayey limestone, and biogenic reefal limestones. Drilling data estimates its thickness at approximately 420 meters in the dam area.

A key structural feature is the Chamshir Syncline, a 12-kilometer-long fold with complex geometry and varying bedding plane orientations due to uplift. The dam is designed with double-curved arches, and its left abutment presents geomorphological challenges, including cliff-like limestone formations 400 meters downstream (Fig. 1). These features increase the potential for water leakage in the left abutment compared to the right one [30].

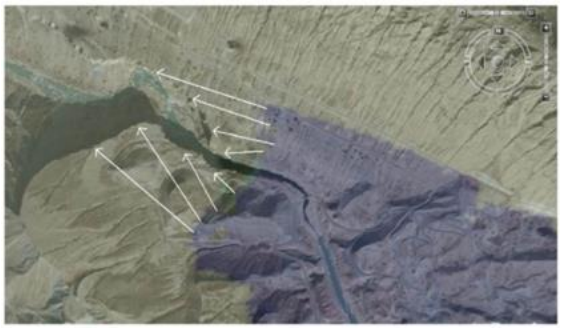

Fig. 1. Morphology of the Chamshir Dam Abutments [30].

3. METHODOLOGY

The left abutment of the Chamshir Dam consists of three main zones: Lower Mishan, Middle Mishan, and the Transition Zone. These zones were selected as key areas for modeling, with data from the Chamshir Dam used as the foundation for the simulations. The mechanical properties of these zones were derived from laboratory tests and field data are presented in Table 1.

For simulating the fracture network in the region, the software 3DEC, which is based on the discrete element method, was employed. This software enables precise modeling of discontinuities in rock masses. Additionally, seepage analysis of the left abutment was conducted using both 3DEC and Seep/w software. Seep/w, a two-dimensional analysis tool based on the finite element method, operates under the assumption of Darcy's law and uses Laplace's equation to simulate fluid flow in porous media.

This combination of numerical modeling tools provides a robust framework for evaluating the seepage behavior in the abutment and assessing the effectiveness of the cutoff wall.

Table 1. Mechanical properties of the Chamshir site

Zone	Lower Mishan	Transmission area	Middle Mishan
Density (Kg/m3)	2430	2570	2560
Poison-ratio	0.31	0.23	0.31
Yang modulus (GPa)	2.5	4.5	7.5
Cohesion (MPa)	6.11	7.3	7.01
Friction angle (Degree)	40	43	45
Tensile strength (MPa)	4.82	5.63	6.03

3.1. Generation of The Discrete Fracture Network

Random fracture network models represent the heterogeneous nature of fractured rock masses as discrete elements with geometrical properties and features defined statistically. These models account for the geometry of fracture networks, intact rock blocks, and the nature of rock bridges between fractures. Among the most effective methods for simulating the stochastic nature of fracture geometrical properties is the three-dimensional stochastic modeling of discrete fracture networks (DFN). The essential geometrical properties required for generating a DFN include orientation (dip and dip direction), trace length, aperture, and the spatial position of the fracture center.

The geometrical properties for generating the DFN were determined based on two-dimensional surveys conducted on the rock mass of the left abutment of the Chamshir Dam. A total of 176 fractures were recorded across both abutments, of which 86 fractures were randomly surveyed on the left abutment. Fig. 2 illustrates the distribution of fracture sets recorded in the left abutment. The orientation of discontinuities follows a Fisher distribution.

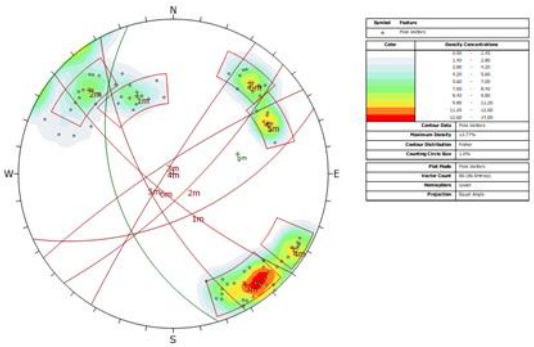

Fig. 2. Distribution of the measured joint sets in the left support.

Ultimately, six fracture sets were identified in the left abutment. The fracture sets J1 and J2, J3

and J4, and J5 and J6 exhibit similar geometrical characteristics. Therefore, the fractures in the left abutment can be categorized into three primary fracture sets.

The log-normal distribution was utilized to generate fracture lengths, as expressed by Eq. (1).

$$PDF(x) = f(x) = \frac{e^{-(\frac{ln\,x-\mu}{\sqrt{2}\sigma})^2}}{x\sqrt{2}\pi\sigma} \quad (1)$$

$\bar{h}log_{log}$**=μ=1.373**

$\sigma_{\log}=\sigma = 0.64125$

In this equation, σ and μ represent the mean and standard deviation of the probability distribution of the fracture lengths, respectively. Additionally, the cumulative probability distribution of fracture lengths is calculated using Eq. (2), where ha and hb denote the lower and upper bounds of the fracture lengths.

$$\int_{h_a}^{h_b} f(H)dH = \frac{1}{2}\left(erf\left(\frac{ln\,h_a - \bar{h}_{log}}{\sqrt{2}\sigma_{log}}\right)\right) \quad (2)$$

Based on numerous past studies and field observations [31, 32], the Poisson distribution is the best fit for the location of fractures. Consequently, the geometric centers of the fractures are generated using random numbers based on a recursive algorithm. The fractional part of the computed numbers is determined by the recursive equation provided in Eq. (3).

$$R_{i+1} = 27R_i - INT(27R_i) \quad (3)$$

R is a random number in the range 0<R<10, and INT generates the integer part of the number within parentheses.

In the three-dimensional simulation of the fracture system, the orientation of each fracture is defined by two parameters: dip and dip direction. The use of the Fisher distribution function to determine the dip angle of fractures is common practice (Eq. (4)) [33]. The Fisher distribution function describes the probability of finding an orientation within an angular range θ from the actual mean.

$$f(\theta) = \frac{ke^{k\,cos(\theta)}}{2\pi(e^k - e^{-k})} \quad (4)$$

Where k is the Fisher constant, which measures the dispersion around the mean dip angle. This distribution function is symmetric about the mean dip and, as expected, has its maximum value at the actual mean (θ=0). The concentration parameter k determines the level of clustering, with larger values indicating greater concentration of the data around the center of the distribution. Using the Fisher distribution, the dip angle of each random fracture can be determined using Eq. (5).

$$\Delta\theta = cos^{-1}\left(\frac{ln(1 - Random(0.1)}{k} + 1\right) \quad (5)$$

Δθ represents the deviation of the fracture dip angle from the mean angle, and Random (0,1) is a uniformly distributed random number between 0 and 1.

Since the creation of a discrete fracture network (DFN) relies on random distribution for generating various fracture features, this randomness can influence the final results and yield different outcomes. To ensure the generated fracture network closely resembles real-world conditions and to minimize errors in permeability estimation, the following assumptions were made: fracture planes are considered disk-shaped, boundary effects are minimized by maintaining a generation space-to-DFN model ratio greater than 4, volumetric intensity (P30) is used for fracture network generation, and immature fractures are excluded. These measures help minimize the random effects of the DFN and improve the reliability of the results.

To evaluate the impact of randomness, three models of the zones at the REV (Representative Element Volume) level were constructed, and different fracture networks were generated using various random numbers. The flow rate for each fracture network was calculated, revealing consistent results across the models. The results demonstrated minimal variation, confirming the robustness of the assumptions. A sample of the generated fracture network and the corresponding flow rate calculations are presented in Fig. 3.

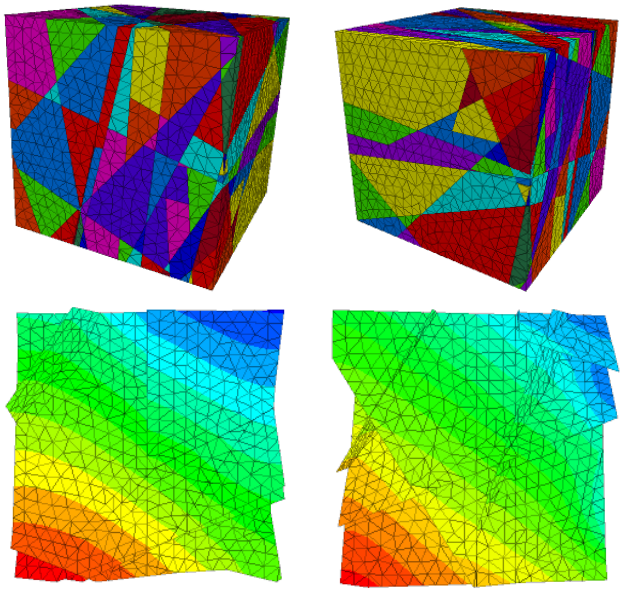

Fig. 3. A sample of the fracture network generated and the determination of the fluid flow through it.

3.2. Hydraulic Calibration Of The Joint Network Using In Situ Experiment Data

To estimate the hydraulic aperture, a back-analysis was conducted by comparing the numerical solution results with the in situ permeability test results. To ensure the numerical model's results align with real-world conditions, the permeability parameters in the model were adjusted until the corresponding permeability in the environment was achieved. Since the Lugeon test was the only test conducted to evaluate permeability in the region, its results were used to calibrate the model.

For this purpose, a large-scale model of each zone, the Representative Elementary Volume (REV) was created, and the flow rate from these models was calculated. By substituting the calculated flow rate into Darcy's law, presented in Eq. (6), the permeability value was obtained. The calculated values were then compared with the in-situ results, and the aperture of fractures in each zone was adjusted to closely match the in-situ values. Consequently, the hydraulic aperture of fractures in each zone was determined. The results are presented in Table 2.

$$Q = K.A(H_1 - H_2)/L \quad \textbf{(6)}$$

The calibration errors and their impact on the model's accuracy were analyzed by comparing the calculated permeability values with the in situ results from the Lugeon tests. Using the mean absolute error (MAE) as a metric, the calibration errors for different zones were determined, with values of 5×10^{-8} for the Lower Mishan, 2.5×10^{-7} for the Transmission area, and 7.2×10^{-7} for the Middle Mishan. Calculated errors were found to be within an acceptable range, ensuring the reliability of the model. The analysis of these errors provided insights into their influence on the model's accuracy, particularly regarding predicted flow rates and hydraulic aperture estimations.

Table 2. Calibration of the hydraulic aperture of fractures using back-calculation analysis by field test results

Zone	In situ permeability (m/s)	Aperture (μm)	Flux (m^3/s)	Numerical permeability (m/s)
Lower Mishan	2.86×10^{-7}	10	7.2×10^{-7}	1.85×10^{-9}
		50	9.15×10^{-5}	2.36×10^{-7}
Transmission area	1.82×10^{-6}	20	5.98×10^{-6}	1.52×10^{-8}
		70	6.16×10^{-4}	1.57×10^{-6}
Middle Mishan	4.03×10^{-6}	72	6.63×10^{-4}	1.69×10^{-6}
		80	9.04×10^{-4}	2.3×10^{-6}
		90	1.3×10^{-3}	3.31×10^{-6}

3.3. Modeling And Applying Cutoff Walls To The Model

The left abutment of Chamshir Dam is 267 meters long and comprises four main zones: Lower Mishan, Middle Mishan, the Transition

Zone, and Upper Mishan. However, due to erosion, the Upper Mishan zone has largely disappeared, leaving only small remnants. Since it does not play a role in the permeability of the site, it has been excluded from the modeling process.

The constructed 3D model was designed to fully encompass the cutoff wall. This model measures 400 meters in length and 100 meters in width. The abutment was created by assembling 100 blocks and connecting them. By applying the site's physical and mechanical properties, the model was divided into three primary zones representing the Lower Mishan, Middle Mishan, and the Transition Zone. Fig. 4 illustrates the constructed model.

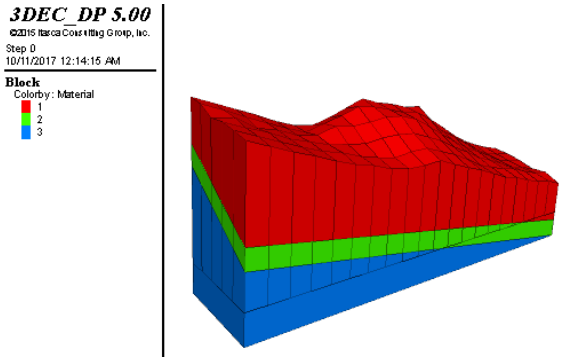

Fig. 4. The model of the zoning situation of the Chamshir site.

To construct the cutoff wall within the injection galleries, the halving method was utilized. Initially, boreholes were drilled and grouted at intervals of 16 meters. Subsequently, additional grouting was carried out at the midpoint between these boreholes, at intervals of 8 meters. This process was repeated at intervals of 4 meters and continued progressively to a spacing of 1 meter. The boreholes were drilled at an angle of 25 degrees to the vertical surface and had a length of approximately 60 meters. The simulated cutoff wall in the model is shown in Fig. 5.

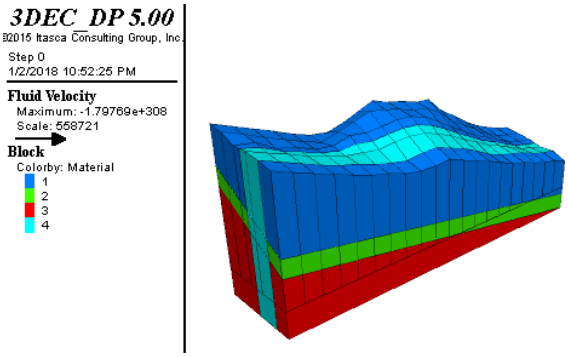

Fig. 5. 3D model showing the zoning of the Chamshir site with the cutoff wall applied.

The hydraulic conditions of the model were implemented by applying pore pressure. The height of the Chamshir Dam is 155 meters, and the water level behind the dam after impoundment reaches 150 meters. Consequently, the pore pressure at the upstream side of the dam after impoundment is calculated to be 1.47×106 Pascal. This pressure was applied as a water pressure gradient at the upstream side of the dam, increasing with depth.

3.4. Evaluation Error Of The Empirical Relationships

Empirical methods provide a simple and quick approach to estimating permeability, which justifies their use. Numerous empirical relationships have been proposed for permeability estimation, but a gap remains in identifying the most suitable empirical method that closely aligns with numerical modeling results and in situ measurements. The efficiency of various empirical relationships was evaluated based on the available in-situ test data, followed by an uncertainty analysis to select the most appropriate method.

Figs. 6-10 illustrate a detailed comparison between permeability values obtained from empirical methods and in-situ Lugeon test results. In most methods and tests, the permeability estimated using empirical methods was found to be lower than the values obtained through in-situ tests, highlighting a discrepancy that suggests these methods may not fully capture actual seepage risks. Empirical formulas often rely on simplified assumptions, overlooking key factors like fractures and joints, assuming geological uniformity, and ignoring local effects such as pressure or flow variations that Lugeon tests can capture more accurately. This limitation could lead to design errors and potentially compromise the stability of structures. To evaluate the accuracy of the empirical methods, the Root Mean Square Error (RMSE) was calculated as a measure of deviation, with lower RMSE values indicating greater alignment between empirical predictions and in situ results. The RMSE is computed using Eq. (7).

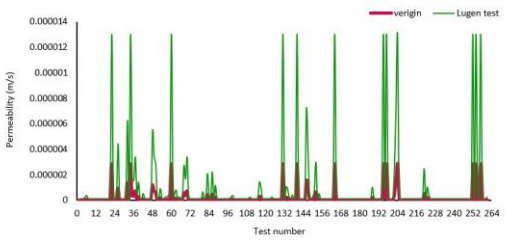

Fig. 6. Comparison of results of the lugeon test with the Verigin method.

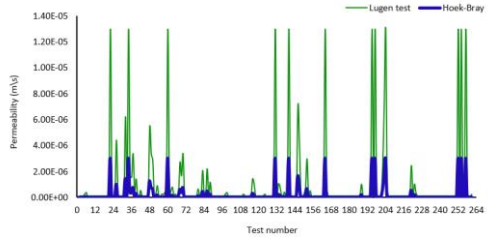

Fig. 7. Comparison of results of lugeon test with Hoek-Bray method.

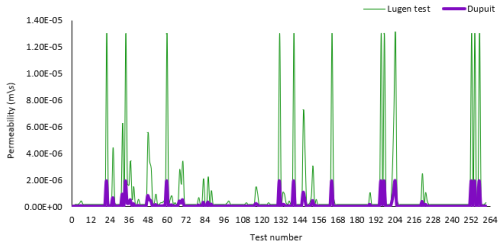

Fig. 8. Comparison of results of the lugeon test with the Dupuit method.

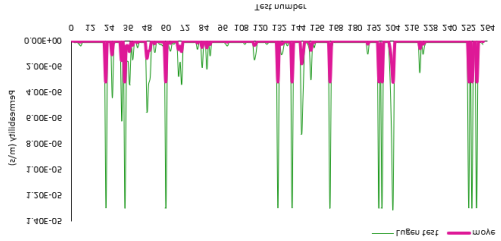

Fig. 9. Comparison of results of lugeon test with Moye method.

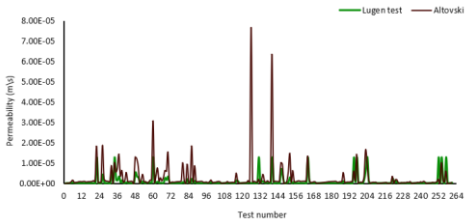

Fig. 10. Comparison of results of lugeon test with Altovski method.

$$RMSE = \sqrt{\frac{\sum_1^N (K - K')^2}{N}} \qquad (7)$$

Where K represents the permeability measured through in-situ tests, K' is the permeability estimated by empirical methods, and N is the number of tests. The obtained RMSE values for the methods are as follows: Dupuit (0.2× 10^-7), Altovsky (1.1× 10^-7), Moye (0.18 × 10^-7), Hoek-Bray (0.15 × 10^-7), and Verigin (0.1 × 10^-7), respectively. The results of the analysis reveal that the Hoek-Bray and Verigin methods show the least deviation from Lugeon test data, as evidenced by their low RMSE values, making them the most reliable empirical methods for predicting permeability at the Chamshir site. On the other hand, the Dupuit and Altovski methods exhibited significant deviations, indicating their limited suitability for this application. The Moye method, while less accurate than Hoek-Bray and Verigin, performed better than Dupuit and Altovski with moderate deviations. This comprehensive evaluation underscores the importance of validating empirical methods against in situ data to ensure reliable permeability estimates for fractured rock masses.

4. RESULTS AND DISCUSSION

To investigate the water seepage rate from the left abutment of the Chamshir Dam, a seepage analysis was conducted using the 3DEC and Seep/w software without considering the cutoff wall. The outflow discharge from the left flank was calculated over a length of 400 meters, and the seepage rate was found to be 1.77×10^{-3} cubic meters per second per meter. Similarly, the seepage rate obtained using the Seep/w software was 2.77×10^{-3} cubic meters per second per meter. Fig. 11. presents the analysis of the left abutment, showing the flow potential lines.

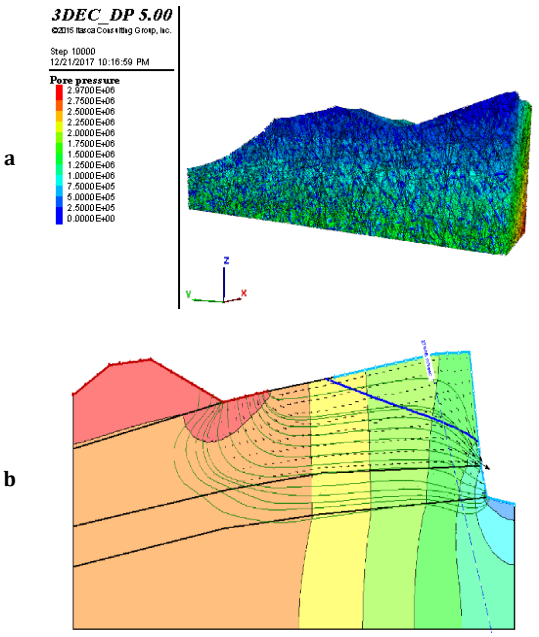

Fig. 11. (a) Analysis of the left abutment of Chamshir Dam without cutoff wall using 3DEC software, (b) Analysis of abutment and condition of flow potential lines using software Seep/w.

Subsequently, the outflow discharge from the downstream side of the dam was calculated, taking into account the cutoff wall, and the effect of the cutoff wall on reducing the outflow was evaluated. The seepage rate determined in this stage using the 3DEC software was 5.79×10^{-4} cubic meters per second per meter. Similarly, the seepage rate obtained using the Seep/w software was 5.46×10^{-4} cubic meters per second per meter.

Thus, the seepage analysis results using the 3DEC software indicate that the implemented cutoff wall reduced the outflow discharge from the left abutment by 70%. Additionally, the Seep/w software showed an 80% reduction in outflow due to the cutoff wall. Fig. 12 presents the seepage analysis of the left abutment with the cutoff wall applied to the model, along with the corresponding flow potential lines.

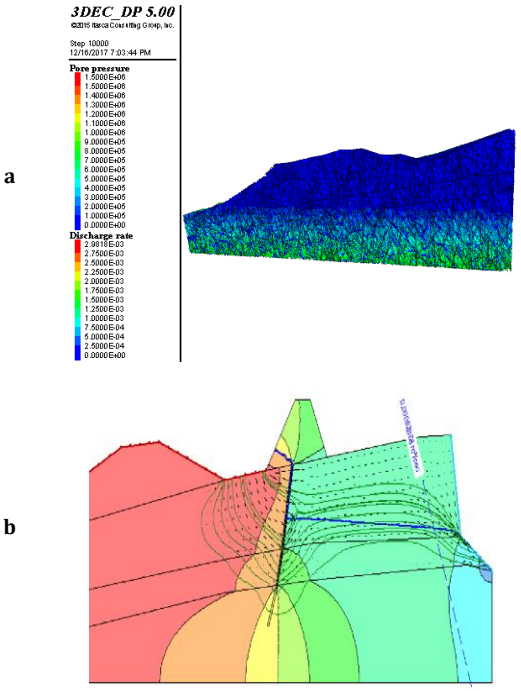

Fig. 12. (a) Analysis of the left abutment of Chamshir Dam by applying the cutoff wall using 3DEC software, (b) Analysis of the abutment of the status of flow potential lines using Seep/w software after applying the cutoff wall.

The RMSE values calculated for the proposed empirical methods, compared to in-situ measurements before the implementation of the cutoff wall, indicate that among the five empirical methods used for estimating permeability, the Hoek method and Verigin method exhibit the lowest error. These methods are therefore considered more suitable for empirical permeability estimation compared to others. Following these, the Moye method showed lower errors than the remaining methods. However, the Dupuit and Altovski methods displayed significant uncertainties compared to the in-situ results, rendering them unsuitable for permeability estimation.

Furthermore, the errors in these methods for predicting the permeability of the cutoff wall were also evaluated by analyzing the deviation in their results after the cutoff wall was applied. Similar to the earlier findings, the Hoek and Verigin methods demonstrated the least errors among all methods, making them the most reliable for permeability estimation. Subsequently, the Moye method showed fewer errors than the others, while the Dupuit and Altovski methods exhibited the highest error levels.

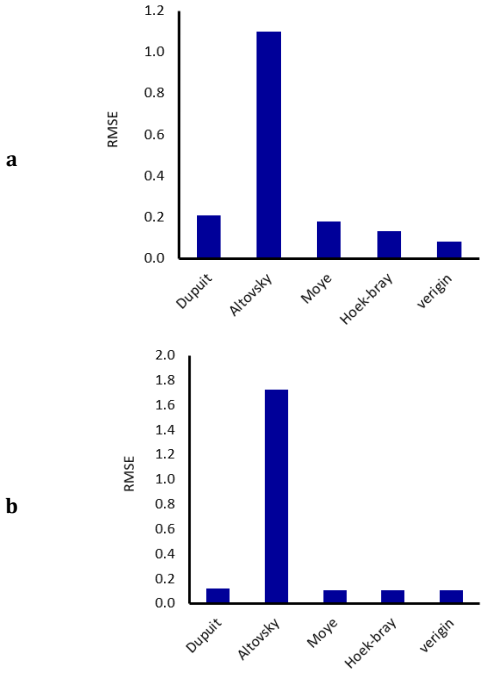

Fig. 13. The RMSE value of empirical relationships: (a) before injection (b) after injection.

5. CONCLUSION

This study highlights the critical role of advanced numerical modeling and empirical validation in designing and assessing seepage control measures for dam structures, focusing on the Chamshir Dam. The results show that implementing a cutoff wall significantly reduces seepage rates, improving structural safety and overall efficiency in fractured rock masses.

Using 3DEC and Seep/w software, seepage behavior was analyzed before and after the cutoff wall. The results demonstrated a seepage reduction of 70% and 80% for the two methods, respectively, confirming their effectiveness in simulating complex seepage mechanisms. Hydraulic calibration using Lugeon test data further ensured model accuracy, with permeability values calculated using Darcy's law and minimal calibration errors across the key geological zones. The study also compared empirical methods for permeability estimation, identifying the Hoek and Verigin methods as the most accurate, based on their low RMSE values. Conversely, methods like Dupuit and Altovski showed significant deviations, limiting their reliability for fractured rock masses.

Seepage rates before the cutoff wall were 1.77×10^{-3} $m^3/s/m$ (3DEC) and 2.77×10^{-3} $m^3/s/m$ (Seep/w), which reduced to 5.79×10^{-4} $m^3/s/m$ and 5.46×10^{-4} $m^3/s/m$ after its application. These results underline the critical role of cutoff walls in mitigating seepage risks. Additionally, three-dimensional modeling of fracture networks provided a comprehensive understanding of flow behavior and validated the robustness of the model.

In conclusion, the study demonstrates the importance of integrating numerical modeling, empirical methods, and field data to optimize seepage control measures. The significant seepage reduction achieved at the Chamshir Dam confirms the efficacy of cutoff walls and the limitations of empirical methods with high uncertainties. This approach offers a practical framework for addressing seepage challenges in fractured rock environments.

Financial support

This work has been supported by the Center for International Scientific Studies & Collaboration (CISSC), Ministry of Science Research and Technology.

REFERENCES

[1] J. Hu and F. Ma, Evaluation of remedial measures against foundation leakage problems of earth dams on pervious conglomerate strata: a case study, Bulletin of Engineering Geology and the Environment, vol. 75, no. 4, pp. 1519–1540, 2016.

[2] M. J. Kazemzadeh-Parsi and F. Daneshmand, Unconfined seepage analysis in earth dams using smoothed fixed grid finite element method, International Journal for Numerical and Analytical Methods in Geomechanics, vol. 36, no. 6, pp. 780–797, 2012.

[3] D. U. Barboza and L. A. Bressani, Seepage Analysis of Concrete and Embankment Dam Abutment: A Case Study of the Ribeirão João Leite Dam, Geotechnical and Geological Engineering, vol. 42, no. 6, pp. 4349-4373, 2024.

[4] E. Wang, J. Zhong, Y. Zhao, and W. Mao, Analysis of seepage and seepage control measures in the rock masses of the Huilong pumped-storage power station, Bulletin of Engineering Geology and the Environment, vol. 74, no. 4, pp. 1453–1462, 2015.

[5] S. Yuan and H. Zhong, Three-dimensional analysis of unconfined seepage in earth dams by the weak form quadrature element method, Journal of Hydrology, vol. 533, pp. 403–411, 2016.

[6] H. K. Shayan and E. Amiri-Tokaldany, Effects of blanket, drains, and cutoff wall on reducing uplift pressure, seepage, and exit gradient under hydraulic structures, International Journal of Civil Engineering, vol. 13, pp. 486-500, 2015.

[7] Y. Li, Y. Chen, Q. Jiang, R. Hu, and C. Zhou, Performance assessment and optimization of seepage control system: A numerical case study for Kala underground powerhouse, Computers and Geotechnics, vol. 55, pp. 306–315, 2014.

[8] T. Jiang, J. Zhang, W. Wan, S. Cui, and D. Deng, 3D transient numerical flow simulation of groundwater bypass seepage at the dam site of Dongzhuang hydro-junction, Engineering Geology, vol. 231, pp. 176–189, 2017.

[9] S. Gao, J. Chai, J. Cao, Z. Xu, Y. Qin, M. Wang, and Y. Chai, Numerical simulation of concrete face rockfill dam seepage: case study of Miaojiaba dam, China, in Proceedings of the Institution of Civil Engineers-Water Management, vol. 174, no. 5, pp. 236–251, 2021.

[10] W. Zhang, Z. Shen, G. Chen, W. Zhang, L. Xu, J. Ren, and F. Wang, Optimization design and assessment of the effect of seepage control at reservoir sites under karst conditions: A case study in Anhui Province, China, Hydrogeology Journal, vol. 29, no. 5, pp. 1831–1855, 2021.

[11] G. Kheiri, H. Javdanian, and G. Shams, A numerical modeling study on the seepage under embankment dams, Modeling Earth Systems and Environment, vol. 6, no. 2, pp. 1075–1087, 2020.

[12] H. F. Aghajani, M. M. Anzabi, Z. Sheikhi, and R. Shokri, Selecting optimum cutoff wall position for rehabilitation of an inclined core earthfill dam, in GeoShanghai International Conference, pp. 252–260, 2018.

[13] M. M. Sazzad and S. Alam, Effect of grout curtain on the seepage characteristics of earth dam by FEM, Journal of Geotechnical Studies, vol. 5, no. 2, pp. 1–10, 2020.

[14] A. Torabi Haghighi, A. Tuomela, and A. A. Hekmatzadeh, Assessing the Efficiency of Seepage Control Measures in Earthfill Dams, Geotechnical and Geological Engineering, vol. 38, no. 5, pp. 5667–5680, 2020.

[15] A. Moharrami, G. Moradi, M. H. Bonab, J. Katebi, and G. Moharrami, Performance of cutoff walls under hydraulic structures against uplift pressure and piping phenomenon, Geotechnical and Geological Engineering, vol. 33, no. 1, pp. 95–103, 2015.

[16] E. Zhao and Y. Jiang, Seepage evolution model of the fractured rock mass under high seepage pressure in dam foundation, Advances in Civil Engineering, vol. 2021, 2021.

[17] H. R. Zarif Sanayei and H. Javdanian, Assessment of steady-state seepage through dams with nonsymmetric boundary conditions: analytical

approach, Environmental Monitoring and Assessment, vol. 192, no. 1, pp. 1–21, 2020.

[18] E. A. F. El-Kasaby, A. A. E. Hegazy, T. H. Nasrallah, and W. H. A. Elkhier, Experimental study of phreatic surface for earth dam with filter, Al-Azhar Univ. Civil Eng. Res. Mag., vol. 41, no. 2, pp. 99–110, 2019.

[19] R. H. Irzooki and A. Jamel, Experimental study of characteristics of top seepage line through homogenous earth dam using Hele-Shaw model, International Review of Civil Engineering (IRECE), vol. 3, no. 6, p. 480, 2012.

[20] K. Mizumura and T. Kaneda, Boundary condition of groundwater flow through sloping seepage face, Journal of Hydrologic Engineering, vol. 15, no. 9, pp. 718–724, 2010.

[21] M. A. Razek, A. A. Salam, and M. Attia, Analysis and Estimation of Seepage Through Earth Dams with Internal Cut Off, 2021.

[22] M. Chouireb, O. N. Noureddine, A. Djehiche, and G. Mostefa, Analysis and Estimation of Seepage through Homogeneous Earth Dams Using Neural Network and Empirical Equation, Advanced Engineering Forum, vol. 49, pp. 79-90, 2023, doi: 10.4028/p-ri07ns.

[23] M. Attia, M. Abdel Razek, and A. A. Salam, Seepage through earth dams with internal cut off, Geotechnical and Geological Engineering, vol. 39, no. 8, pp. 5767–5774, 2021.

[24] X. Tan, X. Wang, S. Khoshnevisan, X. Hou, and F. Zha, Seepage analysis of earth dams considering spatial variability of hydraulic parameters, Engineering Geology, vol. 228, pp. 260–269, 2017.

[25] S.-K. Chen, Q.-D. He, and J.-G. Cao, Seepage simulation of high concrete-faced rockfill dams based on generalized equivalent continuum model, Water Science and Engineering, vol. 11, no. 3, pp. 250–257, 2018.

[26] X. Li, Y. Chen, R. Hu, and Z. Yang, Towards an optimization design of seepage control: A case study in dam engineering, Science China Technological Sciences, vol. 60, no. 12, pp. 1903–1916, 2017.

[27] Y. Xiang, L. Wang, S. Wu, H. Yuan, and Z. Wang, Seepage analysis of the fractured rock mass in the foundation of the main dam of the Xiaolangdi water control project, Environmental Earth Sciences, vol. 74, no. 5, pp. 4453–4468, 2015.

[28] J. Yang, L. Zhao, Z. Shen, L. Gan, and L. Xu, An efficient procedure for optimization design of anti-seepage curtains: a case study, Bulletin of Engineering Geology and the Environment, vol. 80, no. 3, pp. 2671–2685, 2021.

[29] L. Zhang, H. Yang, H. Sun, and Z. Yang, Optimization analysis of seepage control design in Mopanshan Reservoir, northeastern China, Arabian Journal of Geosciences, vol. 13, no. 7, pp. 1–10, 2020.

[30] (2011), Geotechnical reports and studies of the Cham Shir Dam site by Tehran Sahab Consulting Engineers Company (In Persian).

[31] S. D. Priest and J. A. Hudson, Discontinuity spacings in rock, International Journal of Rock Mechanics and Mining Sciences & Geomechanics Abstracts, vol. 13, no. 5, pp. 135-148, 1976/05/01/ 1976.

[32] T. Rives, M. Razack, J.-P. Petit, and K. Rawnsley, Joint spacing: analogue and numerical simulations, Journal of structural geology, vol. 14, no. 8-9, pp. 925-937, 1992.

[33] L. Huang, X. Su, and H. Tang, Optimal selection of estimator for obtaining an accurate three-dimensional rock fracture orientation distribution, Engineering Geology, vol. 270, p. 105575, 2020/06/05/ 2020.

[34] Minárik, M. Reevaluation of Methods for Estimating the Permeability of Selected Slovak Dams.

APPENDIX

Here are concise formulas for seepage analysis based on geological sources and reports related to the Chamshir dam project [30, 34].

Verigin formula:

$$k = \frac{Q\ ln\left(1.47\ \frac{L}{\xi_r r}\right)}{2\pi L p} \tag{1}$$

Where Q water loss [$m^3.s^{-1}$], L length of section[m], p pressure[m], r borehole radius[m] and ξ=2

Dupuit formula:

$$k = \frac{Q\ ln\frac{R}{r_0}}{2\pi L p} \tag{2}$$

Units are like Verigin formula.

Moye formula:

$$k = \frac{Qc}{Lp}\ ,\qquad c = \frac{1 + ln\frac{L}{2r}}{2\pi} \tag{3}$$

Units are like Verigin formula.

Altovski formula:

$$k = 0.525\ Q \log\frac{0.66L}{r} \tag{4}$$

Where Q water loss [$l.min^{-1}.m^{-1}$] by pressure 10 KPa.

Hoek – Bray formula:

$$k = \frac{Q}{p}\frac{\ln\frac{2L\sqrt{\lambda}}{d}}{2\pi L}\ ,\qquad \lambda = \frac{k_x}{k_y} \tag{5}$$

Where Q water loss [$cm^3.s^{-1}m^{-1}$], L length of section[cm], d borehole diameter[cm], p pressure[cm] and λ anisotropy.